Long-lived inert Higgs boson in a fast expanding universe and its imprint on the cosmic microwave background

Dilip Kumar Ghosh,[1,*] Sk Jeesun,[1,†] and Dibyendu Nanda[1,2,‡]

[1]*School of Physical Sciences, Indian Association for the Cultivation of Science, 2A and 2B Raja S. C. Mullick Road, Kolkata 700032, India*

[2]*School of Physics, Korea Institute for Advanced Study, Seoul 02455, Korea*

(Received 23 June 2022; accepted 4 November 2022; published 1 December 2022)

The presence of any extra radiation energy density at the time of cosmic microwave background formation can significantly impact the measurement of the effective relativistic neutrino degrees of freedom or $\Delta N_{\rm eff}$, which is very precisely measured by the Planck Collaboration. Here, we propose a scenario where a long-lived inert scalar, which is very weakly coupled to the dark sector, decays to a fermion dark matter via a "freeze-in" mechanism plus standard model neutrinos at very low temperature $(T < T_{\rm BBN})$. We explore this model in the fast expanding Universe, where it is assumed that the early epoch $(T > T_{\rm BBN})$ of the Universe is dominated by a nonstandard species Φ instead of the standard radiation. In this nonstandard cosmological picture, such late-time decay of the inert scalar can inject some entropy to the neutrino sector after it decouples from the thermal bath and this will make substantial contribution to $\Delta N_{\rm eff}$. Additionally, in this scenario, the new contribution to $\Delta N_{\rm eff}$ is highly correlated with the dark matter sector. Thus, one can explore such *feebly* interacting dark matter particles by the precise measurement of $\Delta N_{\rm eff}$ using the current (Planck 2018) and forthcoming (CMB-S4 and SPT3G) experiments.

DOI: 10.1103/PhysRevD.106.115001

I. INTRODUCTION

The discovery of the 125 GeV Higgs boson by both ATLAS and CMS Collaborations at the LHC completes the basic building blocks of standard model (SM) particle physics, albeit some theoretical and experimental shortcomings. The SM with its present setup is unable to explain the observed nonzero neutrino masses and mixings [1–6] and the existence of dark matter as indicated by various astrophysical and cosmological measurements [7–10]. The resolution of these two fundamental puzzles of particle and astroparticle physics beg for an extension of the SM and a plethora of beyond the standard model (BSM) scenarios have been proposed to address these two issues. The neutrino masses and their mixing angles can be easily accommodated at tree level in the three seesaw mechanisms [11–20]. Note that, in addition to the tree-level seesaw mechanisms, small neutrino masses can also be generated radiatively at one loop level [21,22].

For a very long time, weakly interacting massive neutral particles (WIMPs) [23–28] have been considered as the most coveted candidate for dark matter particles with mass roughly between tens of GeV to a few TeV and sufficiently large (on the order of electroweak strength) interaction with SM particles. WIMPs provide the observed relic abundance $(\Omega h^2 \sim 0.1198)$ via the well-known thermal freeze-out mechanism. Nonobservation of any experimental signal [29–41] of the dark matter (DM) leads to severe constraints on the WIMP paradigm.

To circumvent these constraints on the WIMP scenario, an alternative framework called the freeze-in mechanism has been proposed. In this scenario, the dark matter is a feebly interacting massive particle (FIMP) having highly suppressed interaction strength $\lesssim \mathcal{O}(10^{-12})$ with the SM sector. In the simplest scenario, it is assumed that the initial number density of DM is either zero or negligibly small, and the observed relic abundance is produced nonthermally, either from annihilation or decay of SM particles in the early Universe. The FIMP freezes in once the temperature drops below the dark matter mass and yields a fixed DM relic abundance that is observed at the present day [42–47]. The FIMP, having such a small coupling with the visible sector, can trivially accommodate various null results of DM in different direct detection experiments, such as Panda [29], XENON [30], and LUX [31]. However, FIMP imprints can be traced via cosmological observations such as big bang nucleosynthesis

*tpdkg@iacs.res.in
†skjeesun48@gmail.com
‡dnanda@kias.re.kr

(BBN), cosmic microwave background (CMB), or free streaming length [48–55].

It would be very interesting to look for a minimal BSM paradigm where both the aforementioned sectors (nonzero neutrino mass and FIMP dark matter) are connected. In some particular scenario, such new interactions of neutrinos can have nontrivial implications in cosmological observations and the precision era of cosmological measurements such as BBN or CMB provide us distinctive possibilities for the indirect probe of those hidden particles.

We know that one of the very important and precisely measured observables of the early Universe is the number of effective relativistic neutrino degrees of freedom or $N_{\rm eff}$ which can be changed in the presence of nonstandard interactions of neutrinos. It is usually parametrized as $N_{\rm eff} \equiv (\rho_{\rm rad} - \rho_\gamma)/\rho_{\nu_L}$, where $\rho_{\rm rad}$, ρ_γ, and ρ_{ν_L} are the total radiation energy density, energy density of the photon, and the energy density of a single active neutrino species, respectively. According to the recent Planck 2018 data [10], at the time of CMB formation $N_{\rm eff}^{\rm CMB} = 2.9^{+0.34}_{-0.33}$ with 95% confidence level, whereas the SM predicts it to be $N_{\rm eff}^{\rm SM} = 3.045$ [56–58]. The departure from three, the number of neutrinos in the SM, is the consequence of various nontrivial effects like noninstantaneous neutrino decoupling, finite temperature QED corrections to the electromagnetic plasma and flavor oscillations of neutrinos. So, there is still some room to accommodate the contribution from the beyond SM physics. However, future generation CMB experiments like SPT-3G [59] and CMB-IV [60] are expected to attain a precision of $\Delta N_{\rm eff} \approx 0.06$ at 95% confidence level. Thus, any new contribution to the radiation energy density can be probed very precisely, which can constrain various BSM scenarios that produce light degrees of freedom and are in thermal equilibrium with the SM at early epoch of the evolution of our Universe.

On the other hand, different cosmological events such as decoupling of any relic species from the thermal bath or the nonthermal production of some species are sensitive to the evolution history of the Universe. In the standard cosmological picture, it is assumed that, after the end of the inflation, the energy density of the Universe is mostly radiation dominated (RD). However, we only have precise information about the thermal history of the Universe at the time of BBN ($T_{\rm BBN} \sim$ MeV) and afterward when the Universe was radiation dominated [61,62]. This allows us to consider the possibility that some nonstandard species dominated significantly to the total energy budget of the Universe at early times ($T > T_{\rm BBN}$). In that scenario, if the total energy density is dominated by some nonstandard species, the Hubble parameter (H) at any given temperature is always larger than the corresponding value of H for the standard cosmology at the same temperature. Such a scenario with larger Hubble parameter is known as the fast expanding Universe, where at earlier time (higher temperature) the Universe was matter dominated and eventually at some lower temperature before BBN radiation density ($\rho_{\rm rad}$) takes over the energy density of the nonstandard species ($\rho_{\rm NS}$). One such possibility was discussed in [63] where $\rho_{\rm NS}$ depends on the scale factor as $\sim a^{-(4+n)}$, where $n > 0$. Following the notation of [63], this era of the Universe is identified by temperature T_r, where $\rho_{\rm NS}(T_r) = \rho_{\rm rad}(T_r)$. Thus, the nonstandard cosmological era corresponds to the temperature regime where $T > T_r$. In the limit, $n = 0$ corresponds to the standard radiation dominated cosmological picture. This may be realized by introducing a BSM scalar field Φ with equation of state (EOS) $p_\Phi = \omega\rho_\Phi$, where p_Φ and ρ_Φ denote the pressure and energy density of Φ, respectively, and $\omega \in [-1, 1]$. The energy density prior to BBN redshifts as follows:

$$\rho_\Phi \propto a^{-(4+n)}, \tag{1}$$

where $n = 3\omega - 1$. For $\omega > \frac{1}{3}$ this energy density will fall faster than the radiation. This scenario has been studied in different contexts in the literature [64–69]. We assume this Φ has negligible coupling with the SM sector only so that the only effect it will have is in the expansion rate of the Universe. As the new species redshifts faster than the radiation, its energy density will eventually become subdominant even without the presence of any decay. Several works reported the implications of nonstandard cosmological scenarios in the context of WIMP relic density calculation [63,69–74]. It is observed that, if the thermal DM production occurs before $T_{\rm BBN}$ when the expansion rate of the Universe was larger than the RD Universe, freeze-out happens at an earlier time, thus producing higher relic abundance [70–72]. Thus, one requires larger coupling of the DM with thermal bath particles to produce a higher DM annihilation cross section at the late Universe so that it produces the relic density that matches with the observed one. Similar studies in the case of nonthermal production of DM have also been investigated [69,74,75]. Various phenomenological implications of the nonstandard cosmology have been extensively studied by several groups [76–79].

Motivated by this, we embark on a scenario where the SM particle content is augmented by an inert $SU(2)$ scalar doublet (η) and three SM gauge singlet fermions (N_1, N_2, N_3), where all of them are odd under an unbroken $\mathcal{Z}_2$ symmetry [22,80–87]. The striking feature of this model is the way it connects the origin of the neutrino mass and DM. Neutrino mass can arise through a one loop radiative seesaw, whereas both η^0, the real component of the scalar doublet, and N can be the DM candidate depending on their mass hierarchy. For scalar DM (η^0), different studies [88–91] have shown that the correct relic density can be produced only in the high mass region ($M_{\eta^0} \gtrsim 525$ GeV). However, this scenario can change if we introduce another real gauge singlet scalar S, which is also

odd under $\mathcal{Z}_2$ symmetry and mixes with η^0. The immediate consequence of such nontrivial mixing between the singlet (S) and η^0 is a newly formed scalar DM (η_1) state as a linear superposition of η^0 and S with suppressed gauge interaction compared to the doublet scalar. As a result of this suppressed gauge coupling, the scalar DM can now have mass as low as 200 GeV consistent with the observed relic density [92–94]. However, both in the presence or absence of the singlet scalar, the lightest of the singlet fermions N_i can be a plausible thermal DM candidate due to its Yukawa interaction with a new scalar doublet and the SM leptons. In all such cases, the model faces stringent constraints from different direct detection experiments. As discussed above, motivated by the null results of these experiments, here we study another version of the scotogenic model, where the DM is produced via a nonthermal mechanism. In this analysis, instead of a scalar DM, the lightest singlet $\mathcal{Z}_2$ odd fermion N_1 plays the role of the DM, whereas the lightest neutral scalar (η_1), which is the admixture of the real part of the doublet (η^0) and the singlet (S), is very long-lived and decays to DM plus one neutrino at very late time (after neutrino decoupling). If the decay happens at sufficiently low temperature, after the decoupling of active neutrinos from the thermal bath, it can significantly affect the total radiation energy density of the Universe and contribute to the $\mathrm{N_{eff}}$. While calculating the amount of $\Delta\mathrm{N_{eff}}$, we realized that in the standard cosmological scenario the remnant abundance of η_1 is not sufficient to produce detectable $\Delta\mathrm{N_{eff}}$ in the present experimental sensitivity. We show that the scenario can be significantly changed if our Universe had gone through some nonstandard expansion history.

This paper is organized as follows. Section II is devoted to a brief discussion of the basic setup of the model and important interactions. The discussion on dark matter and $\Delta\mathrm{N_{eff}}$ is presented in Sec. III, while Sec. IV contains our main numerical results. Finally, we conclude in Sec. V.

II. BASIC SETUP

The particle spectrum of this model contains an $SU(2)_L$ inert doublet scalar (η), a real singlet scalar (S), and three right-handed neutrinos N_i, $(i = 1, 2, 3)$ in addition to the SM particles. We impose an additional $\mathcal{Z}_2$ symmetry under which all the SM particles are even, whereas the new fields are odd. In this prescription, the lightest of these $\mathcal{Z}_2$-odd particles will be absolutely stable and be a viable DM candidate. With these particles in hand, one can write down the following interaction Lagrangian:

$$\mathcal{L}_{\text{fermion}} = y_{i\alpha}\overline{\ell_L^i}\,\tilde{\eta}\,N_\alpha + \frac{1}{2}M_{\alpha\beta}\overline{N_\alpha^c}N_\beta + \text{H.c.}, \qquad (2)$$

where ℓ_L^i is the SM left-handed $SU(2)_\mathrm{L}$ lepton doublet, $y_{i\alpha}$ is the lepton Yukawa coupling of flavors $i = e$, μ, and τ, $M_{\alpha\beta}$ is the symmetric Majorana mass matrix, and $\tilde{\eta} = i\sigma_2\eta^*$. The Yukawa interaction, in particular, the y_{i1} term in Eq. (2), plays the most important role in the dark matter phenomenology discussed later in this paper. The scalar potential of the model $V(\phi, \eta, S)$, followed by its minimization condition and relevant mass and coupling parameters, are shown in the Appendix.

After the electroweak symmetry breaking, two neutral physical eigenstates η_1 and η_2 can be expressed as the linear combination of the weak basis η^0 and S as

$$\eta_1 = \cos\theta\eta_0 - \sin\theta S, \qquad (3)$$

$$\eta_2 = \sin\theta\eta_0 + \cos\theta S, \qquad (4)$$

where θ is the neutral CP-even scalar mixing angle. It is obvious that for $\theta = 0$, $\eta_1(\eta_2)$ doublet (singlet) dominated and vice versa for $\theta = \pi/2$. The following parameters describe the scalar sector of this model (see the Appendix for details):

$$M_{\eta_1}, M_{\eta_2}, M_{A^0}, M_{\eta^\pm}, \lambda_\eta, \lambda_S, \lambda_{\phi S}, \lambda_{\eta S}, \lambda_3, \sin\theta. \qquad (5)$$

In addition to these, we also have three right-handed heavy neutrino masses $M_{N_{1,2,3}}$. We use the following mass ordering and the importance of this particular mass pattern in the context of our phenomenology will be discussed shortly:

$$M_{N_3}, M_{N_2}, M_{\eta_2} > M_{\eta_1} > M_{N_1}. \qquad (6)$$

This mass pattern implies that the lightest $\mathcal{Z}_2$-odd fermion N_1 is a suitable candidate for the DM having the Yukawa coupling y_{i1} that features in the production of N_1 from the decay of η_1. To reveal the implications of heavier scalars in our analysis, we consider three distinct values of $M_{\eta^\pm}$, M_{A^0}, and M_{η_2} as represented by three benchmark points BP-1, BP-2, and BP-3 in Table I.

There is an interesting manifestation of relative mass splittings among M_{η_1}, M_{η_2}, and M_{A^0} on the dark matter phenomenology, as well as on constraining the model parameter space from the electroweak precision data. As far as heavier neutrino masses $M_{N_{2,3}}$ are concerned, we set them at $\mathcal{O}(1)$ TeV throughout this analysis so that neutrino masses can be generated radiatively in the right ballpark with $\mathcal{O}(1)$ Yukawa couplings.

Now, a short discussion on the production mechanism of the aforesaid heavy particles and how they remain in

TABLE I. Values of heavy scalar masses for three benchmark points.

	$M_{\eta^\pm}$ (GeV)	M_{A^0} (GeV)	M_{η_2} (GeV)
BP-1	180	250	400
BP-2	150	200	400
BP-3	180	220	500

thermal equilibrium at the early Universe is called for. Both η_1 and η_2 can be produced in the thermal bath of the early Universe through their interactions with the SM gauge bosons and Higgs boson. Heavy neutrinos N_i being a gauge singlet can interact with thermal plasma only through η and their presence in the thermal bath solely depends on the Yukawa interactions as shown in Eq. (2). The DM N_1 is produced nonthermally from the decay of both η_1 and η_2 and the respective decay rates depend on the Yukawa coupling y_{i1} and the corresponding scalar mixing angles $\cos\theta$ and $\sin\theta$. For our choice of benchmark points (see Table I), η_2 mostly decays to $W^{\pm}\eta^{\mp}$ or ZA^0 pairs through gauge interactions, leaving negligible contribution toward N_1 production via Yukawa coupling. Hence, for all practical purposes, $\Gamma(\eta_2 \to \nu + N_1) \simeq 0$. Thus, for our choice of η_1 and N_1 masses, N_1 will be produced in association with active neutrinos from the decay of η_1 (see Fig. 1) with 100% branching ratio, and the corresponding decay width for one neutrino generation can be written as

$$\Gamma_{\eta_1 \to \bar{\nu} N_1} = \frac{y_{N_1}^2 \cos^2\theta M_{\eta_1}}{16\pi}\left(1 - \frac{M_{N_1}^2}{M_{\eta_1}^2}\right)^2, \tag{7}$$

where we denote the Yukawa coupling y_{i1} as y_{N_1} and will use this notation in rest of the paper. From the functional dependence of η_1 decay width [Eq. (7)] on y_{N_1} it is clear that for the late-time production of N_1 from the decay of η_1 via freeze-in mechanism, the Yukawa coupling (y_{N_1}) has to be extremely weak, unlike for the other two heavy neutrinos (N_2 and N_3) that have $\mathcal{O}(1)$ Yukawa interactions with η.

In the presence of such large Yukawa couplings, both N_2 and N_3 will be produced in thermal equilibrium in the early epoch of the Universe and will decay to other lighter $\mathcal{Z}_2$-odd particles (η_1, η_2, $\eta^{\pm}$, and A^0) after their decoupling from the thermal plasma. Hence, these decays would have no impact in the relic abundance of N_1. So far, we were silent about the production of neutrinos in association with N_1 from the decay of long-lived η_1 and its impact on the dynamics of cosmology. The Yukawa coupling (y_{N_1}) is such that the decay $\eta_1 \to N_1 + \nu$ mostly happens after neutrinos decouple from the thermal bath and the decay must also be completed before CMB formation ($T \approx 1$ eV) so that the produced neutrinos in this mechanism have very intriguing implications in the observation of the CMB radiation. To fulfill this condition of η_1 decay, y_{N_1} cannot take any arbitrary value, rather it should be in the range $(\sim 10^{-15}$–$10^{-12})$ as considered in our analysis. As a result, this decay will inject entropy to the neutrino sector only and will increase the total radiation energy density of the Universe at that epoch. However, any significant increment of total radiation energy density during CMB formation will directly impact $\Delta N_{\rm eff}$, as discussed earlier and can be observed in different experiments. The same decay will also set the observed relic density of DM in today's Universe. Hence, the DM mass will decide the amount of energy that gets transferred to the neutrino sector and can directly be related to $\Delta N_{\rm eff}$. The most important parameters of our discussion are M_{η_1}, λ_3, $\lambda_{\phi S}$, $\sin\theta$, M_{N_1}, and y_{N_1}. Among these parameters, M_{η_1}, λ_3, and $\lambda_{\phi S}$ decide the annihilation cross sections of η_1, and $\sin\theta$ decides the mixing of the CP-even real scalars η^0 and S. At the completion of η_1 decay, the final abundance of physical state η_1 gets distributed into DM abundance and active neutrino energy density depending on M_{N_1} and y_{N_1}, thus providing a connection between the DM mass (M_{N_1}) and $\Delta N_{\rm eff}$, and we will explore this in our current endeavor. As we prefer an enhanced comoving number density of η_1 in the mass regime $M_{\eta_1} \gtrsim 60$ GeV, various coannihilation processes between dark sector particles must be suppressed in order to avoid any additional enhancement of effective cross section of η_1, as this would lead to lower abundance of the comoving number density of η_1. The lower yield of η_1, in turn, produces lower neutrino number density and this may not be sufficient to induce an observable effect on $\Delta N_{\rm eff}$. Hence, we suppress the above coannihilation processes by increasing mass splittings between M_{η_1} and other relevant heavy scalar particles of the dark sector. This justifies our choice of associated heavy scalar masses for three benchmarks (BP-1–BP-3) as shown in Table I.

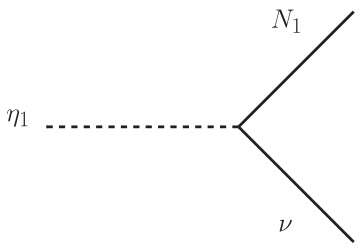

FIG. 1. Feynman diagram corresponding to the decay of η_1.

III. FREEZE-IN DM AND $\Delta N_{\rm eff}$ AT CMB

Following our detailed discussions in previous sections, hereby we address the issue of dark matter (N_1) abundance created by the late-time $(\tau_{\eta_1} > t_{\rm BBN})$ decay of $\eta_1 \to N_1 + \nu$. Since N_1 is the dark matter particle, it must satisfy the observed relic abundance at the present time. To estimate it, one has to solve the following two coupled Boltzmann equations that showcase the evolution of comoving number densities Y_{η_1} and Y_{N_1}, corresponding to η_1 and N_1, respectively, with the temperature of the Universe:

$$\frac{dY_{\eta_1}}{dx} = -\frac{s}{H(x)x}\left(1 - \frac{1}{3}\frac{d\ln g_s(x)}{d\ln x}\right)\langle\sigma v\rangle_{\rm eff}(Y_{\eta_1}^2 - (Y_{\eta_1}^{eq})^2) - \frac{\langle\Gamma_{\eta_1 \to N_1\nu}\rangle}{H(x)x}\left(1 - \frac{1}{3}\frac{d\ln g_s(x)}{d\ln x}\right)Y_{\eta_1}, \tag{8}$$

$$\frac{dY_{N_1}}{dx} = \frac{\langle \Gamma_{\eta_1 \to N_1 \nu} \rangle}{H(x)x} \left(1 - \frac{1}{3}\frac{d\ln g_s(x)}{d\ln x}\right) Y_{\eta_1}, \tag{9}$$

where $x = M_{sc}/T$ is a dimensionless variable with M_{sc} as some arbitrary mass scale that does not affect the analysis, and we consider it to be 100 GeV. Moreover, $Y_{\eta_1}^{eq}$ is the equilibrium comoving number density of η_1, and $g_s(x)$ and $H(x)$ represent the effective relativistic degrees of freedom related to the entropy density and the expansion rate of the Universe, respectively. The thermal average of the effective annihilation cross section of η_1 to the bath particles is denoted by $\langle \sigma v \rangle_{\rm eff}$. The entropy density s and Y_i's are related as $Y_i = \frac{n_i}{s}$ where n_i's are the respective number densities. Finally, $\langle \Gamma_{\eta_1 \to N_1 \nu} \rangle$ denote the thermal average of the decay width given in Eq. (7). While doing our numerical calculation, we take into account all three active neutrinos in $\langle \Gamma_{\eta_1 \to N_1 \nu} \rangle$.

The evolution equation of the comoving number density of η_1 is represented by Eq. (8). The first term on the right-hand side of this equation corresponds to the self-annihilation of η_1 into the SM sector and vice versa, which keeps η_1 in thermal equilibrium. However, in the presence of a tiny Yukawa coupling, η_1 slowly decays into $N_1 + \nu$, thus diluting its number density. This feature is reflected in the second term of Eq. (8). Once the DM (N_1) is produced in the above decay channel, its thermal evolution is governed by Eq. (9). Note that, in the absence of the Yukawa interaction, η_1 becomes stable and plays the role of the DM, having no effect on $\Delta N_{\rm eff}$, and thus it is not considered in this analysis.

We will now discuss the phenomenological consequence of late-time decay of η_1 into DM and neutrinos which is the motivation of this work. The sufficient production of active neutrinos after it decouples from the thermal bath ($T \lesssim 2$ MeV) can hugely affect the total radiation energy density of the Universe at that time and will finally increase $\Delta N_{\rm eff}$. The effective number of relativistic neutrinos at the time of CMB can be written as

$$N_{\rm eff}^{\rm CMB} = \frac{8}{7}\left(\frac{11}{4}\right)^{4/3} \frac{\rho_\nu}{\rho_\gamma}\bigg|_{T=T_{\rm CMB}}, \tag{10}$$

where ρ_ν and ρ_γ are the energy densities of neutrinos and photons, respectively. The production of ν's from some external source will increase its energy density and we parametrize the deviation from the SM value in the following way:

$$\frac{N'_{\rm eff}}{N_{\rm eff}^{\rm SM}} = \frac{\rho'_\nu}{\rho_\nu^{\rm SM}}\bigg|_{T=T_{\rm CMB}}, \tag{11}$$

where ρ'_ν is the total energy density of neutrinos, i.e., the sum of the SM contribution ($\rho_\nu^{\rm SM}$) and the nonthermal contribution ($\rho_\nu^{\rm extra}$) coming from the decay of η_1. Hence, $\Delta N_{\rm eff}$ can be expressed as follows:

$$\Delta N_{\rm eff} = \left(\frac{\rho'_\nu}{\rho_\nu^{\rm SM}} - 1\right) N_{\rm eff}^{\rm SM}\bigg|_{T=T_{\rm CMB}}. \tag{12}$$

To know the temperature evolution of the total neutrino energy density ρ'_ν after the decay of η_1, we need to solve the following Boltzmann equation:

$$\frac{d\rho'_\nu}{dx} = -\frac{4\beta(T)\rho'_\nu}{x} + \frac{1}{xH(x)}\langle E\Gamma \rangle_{\eta_1 \to N_1 \nu} Y_{\eta_1} s, \tag{13}$$

where $\beta(T)$ shows the variation of $g_s(T)$ with T and is defined as

$$\beta(T) = 1 + \frac{1}{3}\frac{T}{g_s(T)}\frac{dg_s(T)}{dT}, \tag{14}$$

and the $\langle E\Gamma \rangle_{\eta_1 \to N_1 \nu}$ term associated with the thermal average of energy density transferred to the neutrino sector from η_1 decay is defined as [95]

$$\langle E\Gamma \rangle_{\eta_1 \to N_1 \nu} = \frac{|\mathcal{M}|^2_{\eta_1 \to N_1 \nu}}{32\pi}\frac{(m_{\eta_1}^2 - m_{N_1}^2)}{m_{\eta_1}^2}\left(1 - \frac{m_{N_1}^2}{m_{\eta_1}^2}\right). \tag{15}$$

The first term on the right-hand side of Eq. (13) shows the dilution of ρ'_ν due to expansion of the Universe, whereas the second term shows the enhancement of ρ'_ν with x after the decay of η_1. The evolution of $\rho_\nu^{\rm SM}$ after neutrinos decouple from the thermal bath can be easily obtained by setting the term proportional to Y_{η_1} of Eq. (13) to be zero ($\rho'_\nu = \rho_\nu^{\rm SM}$), which dictates the dilution of energy density due to expansion only.

From Eq. (13) it is well understood that the total energy density of neutrinos ($\rho_{\nu'} = \rho_\nu^{\rm SM} + \rho_\nu^{\rm extra}$) is decided by the comoving number density (Y_{η_1}) of η_1 after it freezes out. The freeze-out abundance of η_1 depends on its interaction with the bath particles and the expansion rate of the Universe. Freeze-out of η_1 occurs at the temperature where the expansion rate H is greater than the interaction rate ($\langle \sigma v \rangle$). Y_{η_1} decreases if the freeze-out happens at late time equivalently at lower temperature, thus making the Hubble parameter an important quantity that determines the abundance Y_{η_1}.

In the standard cosmology, where it is assumed that the Universe at the time of DM freeze-out is radiation dominated, the corresponding Hubble parameter (H) is defined as

$$H(T) = \sqrt{\frac{8\pi G \rho_{\rm rad}(T)}{3}}, \tag{16}$$

where G is the gravitational constant and $\rho_{\rm rad}(T)$ is the radiation energy density which scales as $\sim T^4$. It turns out that for the range of M_{η_1} considered in our analysis the standard radiation dominated Universe gives $\Delta N_{\rm eff}$ far below the current experimental sensitivity. This is due to the sizable interactions of η_1 with the SM bath, in other

words large $\langle\sigma v\rangle_{\rm eff}$, that keeps η_1 in thermal equilibrium for sufficiently longer duration. Such a large annihilation cross section of η_1 naturally produces low freeze-out abundance Y_{η_1} as $Y_{\rm F.O.} \propto 1/\langle\sigma v\rangle_{\rm eff}$. Hence, the number density of neutrinos produced from such a low yield η_1 is not sufficiently large enough to make any significant changes in $\Delta {\rm N}_{\rm eff}$ that can be measured with current experimental precision. Interestingly, the situation changes drastically if we consider some nonstandard species Φ that dominate the total energy budget of the Universe at early epoch, where the Universe goes through faster expansion at the time of η_1 freeze-out. Here one assumes that, in the pre-BBN era, the energy density of the Universe receives contributions from both the radiation as well as a new species Φ. The energy density of Φ scales as $\sim a^{-(4+n)}$ for $n > 0$ and can be rewritten in the following form:

$$\rho_\Phi(T) = \rho_\Phi(T_r)\left[\frac{g_s(T)}{g_s(T_r)}\right]^{(4+n)/3}\left(\frac{T}{T_r}\right)^{(4+n)}, \quad (17)$$

where g_s is the effective degrees of freedom contributing to the entropy density. We consider T_r as the temperature where $\rho_\Phi = \rho_{\rm rad}$. Thus, using the entropy conservation law, one can express the total energy density $[\rho(T) = \rho_\Phi(T) + \rho_{\rm rad}(T)]$ at a given temperature T in the following form [63]:

$$\rho(T) = \rho_{\rm rad}(T)\left[1 + \frac{g_\rho(T_{\rm r})}{g_\rho(T)}\left(\frac{g_s(T)}{g_s(T_{\rm r})}\right)^{\frac{4+n}{3}}\left(\frac{T}{T_{\rm r}}\right)^n\right], \quad (18)$$

where g_ρ is the effective relativistic degrees of freedom. For $T > T_{\rm r}$ the energy budget of the Universe is dominated by Φ. The Hubble parameter H in Eq. (16) is now determined by the total energy density $\rho(T)$ as shown in Eq. (18) instead of only $\rho_{\rm rad}(T)$. Note that the $n = 0$ limit recaptures the standard cosmological picture. Hence, T_r and n are the two important parameters that decide the expansion rate H. For $n > 0$ the expansion rate of the Universe at a given temperature T is always larger than the corresponding value in the standard radiation dominated ($n = 0$) scenario. As a result of this fast expansion, the condition $\langle\sigma v\rangle_{\rm eff} < H(x)$ is achieved earlier and η_1 freezes out at temperature T higher than than the corresponding temperature in the standard cosmological picture. With such an earlier freeze-out, the abundance Y_{η_1} is large enough to significantly increase the amount of $\Delta_{\rm N_{eff}}$ in our proposed model. However, one should be careful of the potential impact of the above phenomena on the successful predictions of light element abundance by the BBN. If T_r is close to BBN temperature $T_{\rm BBN} \sim 1$ MeV, the Universe starts to expand faster than the radiation dominated picture around $t_{\rm BBN}$ and this may modify the theoretical prediction for BBN abundances. To avoid this, $T_{\rm r}$ must satisfy the following condition [63]:

$$T_{\rm r} \gtrsim (15.4)^{\frac{1}{n}}\ {\rm MeV}. \quad (19)$$

Up to this point, we were silent about the nature of Φ or the essential potential that can give rise to expansion faster than the usual RD Universe and treated n and T_r as free parameters. Followed by the discussion in the Introduction, we assume Φ to be a scalar field that is minimally coupled to gravity with a positive self-interacting scalar potential $[V(\Phi)]$. The EOS parameter (ω) lies in the range $\omega \in [-1, 1]$, i.e., $n \in [-4, 2]$ depending on whether the potential energy $V(\Phi)$ or kinetic energy (KE) term dominates [65,96,97]. The former situation is realized if Φ is oscillating about the minimum of a positive potential [65] and has been studied in different contexts [98–101]. On the other hand, the scenario where the Universe's energy density is dominated by the KE of the scalar field gives rise to the later one ($n = 2$), which is often known as kination [64,66–68]. Such theories with $n = 2$ are realizations of the quintessence fluids motivated to explain accelerated expansion of the Universe [102–104]. However, in this work, we are interested to study how the fast expanding Universe enhances the abundance Y_ϕ as well as $\Delta {\rm N}_{\rm eff}$ for any $n > 0$.

In the next section, we will discuss comprehensive numerical analysis of relic density calculation along with $\Delta {\rm N}_{\rm eff}$ and its phenomenological implications. While doing our numerical analysis, we will vary parameters T_r and n such that they satisfy Eq. (19).

IV. NUMERICAL RESULTS

In the previous section, we have argued that if some nonstandard matter field Φ dominates the total energy budget of the Universe at early epoch, the Universe goes through a faster expansion and η_1 freezes out early with sufficiently large relic abundance. From η_1 the dark matter (N_1) and neutrinos are produced via a freeze-in mechanism. Thus, the produced number density of neutrinos is sufficiently large enough to make a substantial new contribution to $\Delta {\rm N}_{\rm eff}$ which can be verified in the current experiment. In this section, we will scan our model parameter space to quantify this modified $\Delta {\rm N}_{\rm eff}$. We will also show that, for a given set of model parameters, $\Delta {\rm N}_{\rm eff}$ is highly correlated with the dark matter mass M_{N_1}. Any direct experimental verification of FIMP-like dark matter is extremely challenging due its tiny coupling with the SM sector. However, in this scenario, we find that the observed value of $\Delta {\rm N}_{\rm eff}$ is strongly dependent on M_{N_1} and one can utilize this observable as an experimental probe for FIMP-like dark matter. The presence of additional scalars [$SU(2)$ doublet and a singlet] and three generations of heavy neutrinos can have important implications on various existing experimental data. Hence, to have a phenomenologically consistent model, it is necessary to carefully scrutinize the aforementioned BSM scenario in light of those

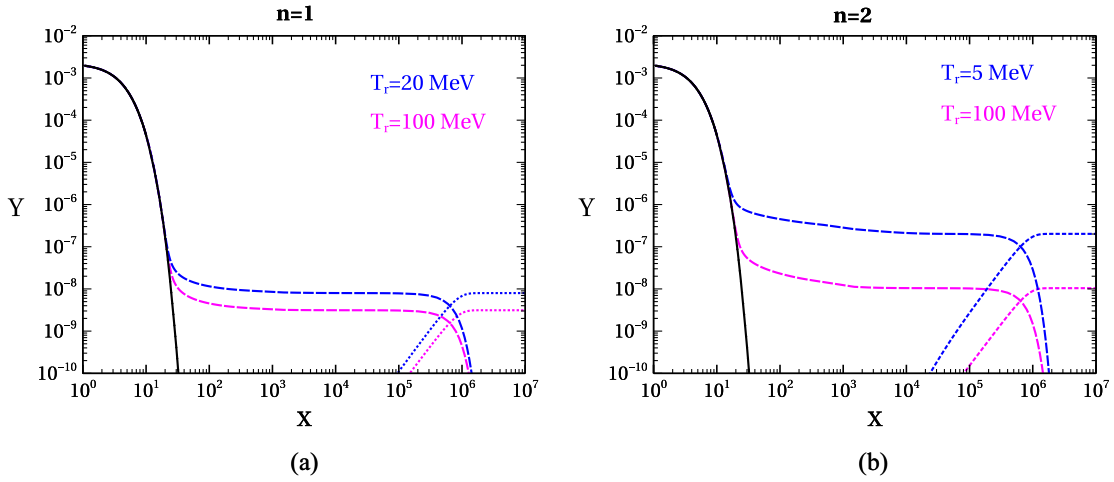

FIG. 2. Evolution of comoving number densities of η_1 and N_1 as a function of dimensionless variable x for $\lambda_3 = 10^{-3}$, $\lambda_{\phi S} = 10^{-3}$, $M_{N_1} = 10$ MeV, $M_{\eta_1} = 65$ GeV, $y_{N_1} = 10^{-12}$, $\sin\theta = 0.9$. Solid, dashed, and dotted lines correspond to $Y^{eq}_{\eta_1}$, Y_{η_1}, and Y_{N_1}, respectively. Comoving number densities are shown for different values of T_r for (a) $n = 1$ and (b) $n = 2$.

experimental data. In addition to these, mathematical consistency of the scenario also demands that various model parameters must satisfy certain theoretical conditions. However, for the brevity of the analysis, we will not discuss these here; nevertheless, further details can be seen in [92]. We will first discuss the full numerical solutions to the Boltzmann equations corresponding to Y_{η_1} Eq. (8) and Y_{N_1} Eq. (9), respectively. For this analysis, we first implement the interactions, mass, and mixings of the model in FeynRules [105], that generate required CALCHEP [106] model files for micrOMEGAs [107] to calculate a thermally averaged cross section $\langle\sigma v\rangle_{\rm eff}$. To showcase the behavior of Y_{η_1} and Y_{N_1} with temperature T, we consider $M_{\eta_1} = 65$ GeV,[1] $M_{N_1} = 10$ MeV, $\lambda_3 = 10^{-3}$, $\lambda_{\phi S} = 10^{-3}$, $\sin\theta = 0.9$, and the Yukawa coupling $y_{N_1} = 10^{-12}$. It is worth pointing out that those parameters are consistent with all theoretical and experimental constraints discussed earlier. We have two additional parameters T_r and n that fix the cosmological framework of our present scenario. The comoving number densities Y_{η_1} and Y_{N_1} for η_1 and N_1 are plotted as a function of x for $n = 1$ [Fig. 2(a)] and $n = 2$ [Fig. 2(b)], respectively.

In Fig. 2(a), blue and magenta lines correspond to $T_r = 20$ and 100 MeV, while in Fig. 2(b) the corresponding two colored lines represent $T_r = 5$ and 100 MeV, respectively. From Eqs. (16) and (18) one can find that, in the presence of an extra contribution to the energy density of the Universe, the Hubble parameter H goes like $\sim T^2(T/T_r)^{n/2}$, $(T \gg T_r)$ and this explains why the expansion rate of the Universe increases with the increase in n (for $n > 0$), which ultimately leads to an earlier freeze-out of η_1 with higher abundance. This feature of a fast expanding Universe is nicely evinced in both Figs. 2(a) and 2(b), where comoving number densities for η_1 as well as N_1 are higher for $n = 2$ compared to $n = 1$ for a fixed $T_r = 100$ MeV (magenta lines). It is clearly evident from Fig. 2 that η_1 decouples from the thermal bath first and then decays into $N_1 + \nu$ at some later time, which basically increases the dark matter comoving number density Y_{N_1}. In addition, one can also notice from Fig. 2 that, for a fixed n, Y_{η_1} decreases with the increase in T_r and this can be once again traced back to the parametric dependence of the Hubble parameter H on T_r and n as mentioned earlier. In summary, both Y_{η_1} and Y_{N_1} increase with an increase in n for a given T_r, while they decrease with an increase in T_r for any value of $n \geq 1$. Interestingly, both of these observations can be interpreted in terms of the modified Hubble parameter $H(T)$ in the fast expanding Universe.

After illustrating the importance of the fast expanding Universe in the calculation of relic abundances for both η_1 and N_1, we now scan the independent parameters of the model in the following range:

$$\lambda_3 \in [10^{-6}:\ 10^{-2}], \qquad \lambda_{\phi S} \in [10^{-6}:10^{-2}], \tag{20}$$

$$M_{\eta_1} \in [50:100\ \text{GeV}], \qquad M_{N_1} \in [1:1000\ \text{MeV}], \tag{21}$$

$$\sin\theta \in [0.0:0.9]. \tag{22}$$

The purpose of this scan is to find a region in the multidimensional model parameter space that is allowed by both theoretical and experimental constraints as well as satisfy the correct relic density [92,108–111]. We will then use those allowed parameters to calculate the value of $\Delta N_{\rm eff}$ in our model that can be substantiated in the upcoming experiments. Throughout this analysis, we fix the mass of the SM-like Higgs to 125 GeV. One can notice that we vary $\sin\theta$ in the above range (0.0–0.9) so that we can capture the

[1]For this value of M_{η_1}, $h \to \eta_1\eta_1$ is kinematically forbidden and hence no constraints from $\text{BR}_h \to \text{inv}$.

effect of both the $SU(2)$ doublet η^0 and singlet S scalars in the freeze-in production of the DM in η_1 decay, where the heavy scalar η_1 becomes doublet (singlet) dominated for $\sin\theta = 0(0.9)$. For this analysis, we fix $n = 2$, $T_r = 5$ MeV, and the Yukawa coupling $y_{N_1} = 10^{-12}$. Varying the Yukawa coupling in the range as mentioned in Sec. II will have no impact on relic density because

$$\Omega_{\rm DM}h^2 = 2.755 \times 10^8 Y_{\rm DM} \frac{M_{\rm DM}}{\rm GeV},$$

and $Y_{\rm DM}$ will always be the same as $Y_{\eta_1}(x_{f.o.})$. At the end, the parameter scan result in the $M_{\eta_1} - \sin\theta$ plane is visible in Fig. 3, where DM mass M_{N_1} is represented by the color bar. As one can observe, a significant region of the parameter space in Fig. 3 has been excluded by various theoretical and experimental constraints. The $\mathrm{Br}(h \to \mathrm{inv}) < 11\%$ excludes the region with $M_{\eta_1} < M_h/2$ and this is the gray colored vertical patch marked as $\mathrm{Br}(h \to \mathrm{inv}) > 11\%$ [111]. The electroweak precision data (EWPD) through S, T, and U parameters serve another crucial limit on the parameter space of this model. It is well known that the larger the mass splitting between the components of the $SU(2)$ doublet field, the stronger is the EWPD constraints [92]. Indeed, this is happening in the case of our three benchmark points shown in Table I. The EWPD data exclude three diagonal bands corresponding to BP-1, BP-2, and BP-3, respectively, in Fig. 3. From this figure, it is clear that BP-3, which has the largest mass gap between M_{η_2} and $M_{\eta^\pm}$, attracts the strongest EWPD limit and it excludes $\sin\theta \lesssim 0.6$–0.775 for $M_{\eta_1} \approx 62.5$ GeV and $\sin\theta \lesssim 0.6$–0.75 for $M_{\eta_1} = 100$ GeV. Thus,

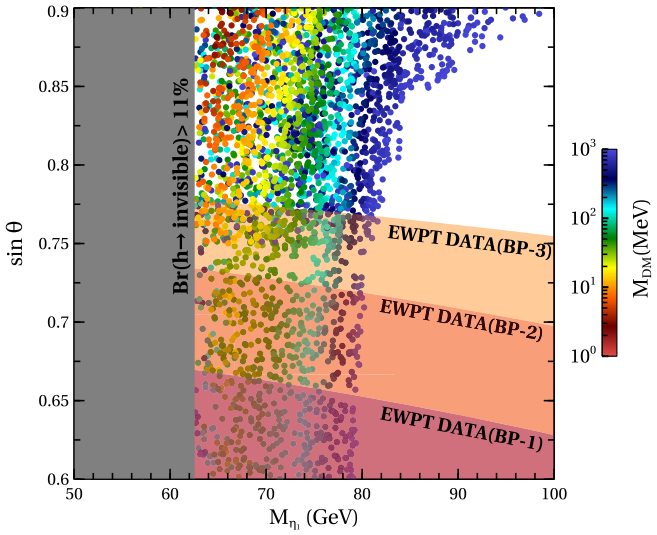

FIG. 3. The allowed parameter space from the electroweak precision test (EWPT) data and Higgs's invisible decay width constraints in $\sin\theta - \mathrm{M}_{\eta_1}$ plane for $10^{-6} \le \lambda_3 \le 10^{-2}$, $10^{-6} \le \lambda_{\phi S} \le 10^{-2}$, $y_{N_1} = 10^{-12}$, $n = 2$, $T_r = 5$ MeV. Here the color bar shows the variation of DM mass.

the overall allowed region is located at the upper quadrilateral part of the parameter space, with $\sin\theta \sim 0.775$–0.9 and $M_{\eta_1} \sim 62.5$–100 GeV. Another important outcome of our analysis is that for a fixed $\sin\theta$ any increase in M_{N_1} also calls for an increase in M_{η_1} to satisfy the correct density and Fig. 3 perfectly corroborates our claim. However, one has to look for any physical processes that may imperil the effect of the long-lived scalar on CMB in the singlet-doublet scotogenic model. In this scenario, the presence of other heavy scalars may lead to DM coannihilation processes that may boost the $\langle\sigma v \gtrsim\rangle_{\rm eff}$ and such enhanced $\langle\sigma v\rangle_{\rm eff}$ ultimately suppresses η_1 abundance. The immediate consequence of this low yield η_1 is the tiny production of an additional neutrino density ρ'_ν that may not lead to any significant shift in $\Delta\mathrm{N}_{\rm eff}$, thus spoiling the intention of this analysis. The most natural way to circumvent this situation is to take other particles of the model very heavy compared to M_{η_1} (large mass splittings) so that one can easily ignore the coannihilation of η_1 with those heavier particles. To facilitate this, in our analysis we choose three representative benchmark points (BP-1–BP-3) as shown in Table I.

After having a suitable model parameter space consistent with various constraints, we are now in a position to kick off the numerical estimation of the ratio $\rho'_\nu/\rho^{\rm SM}_\nu$. For this we need to solve Eqs. (8) and (13) to evaluate the evolution of $\rho'_\nu/\rho^{\rm SM}_\nu$ as a function of the dimensionless variable x. In Fig. 4(a) we display the dependence of $\rho'_\nu/\rho^{\rm SM}_\nu$ as a function of x for three different values of M_{η_1} (65 GeV, solid cyan line; 67 GeV, brown dot-dashed line; 70 GeV, blue dashed line) where the other parameters are kept fixed ($\lambda_3 = 10^{-3}$, $\lambda_{\phi S} = 10^{-3}$, $M_{N_1} = 10$ MeV, $\sin\theta = 0.9$, $n = 2$, $T_r = 5$ MeV) for a constant Yukawa coupling $y_{N_1} = 10^{-12}$. From Fig. 4(a) one can clearly discern that, at very high temperature T, η_1 stays in thermal equilibrium for $M_{\eta_1} = 65$ GeV with no additional contribution to ρ'_ν from η_1, thus the ratio $\rho'_\nu/\rho^{\rm SM}_\nu$ is almost unity. However, as the Universe starts cooling, the decay $\eta_1 \to N_1 + \nu$ also proceeds through tiny Yukawa coupling y_{N_1} and it leads to new contributions to the neutrino energy density. This additional contribution makes the ratio $\rho'_\nu/\rho^{\rm SM}_\nu$ greater than 1. The decay of η_1 continues until its number density is completely converted into N_1 and ν number densities. At that point, no further neutrinos are generated and the $\rho'_\nu/\rho^{\rm SM}_\nu$ saturates. This feature is repeated for the other two values of $M_{\eta_1} = 67$ and 70 GeV in Fig. 4(a) with a marked difference. For a higher value of M_{η_1}, the thermally averaged cross section $(\langle\sigma v\rangle)_{\rm eff}$ of η_1 with SM particles increases due to larger phase space availability. This elevated cross section leads to the late-time freeze-out of η_1 with smaller abundance. Subsequently, the late-time decay of η_1 produces neutrinos with suppressed energy density [92]. From this analysis, we conclude that, for a fixed value of x, the ratio $\rho'_\nu/\rho^{\rm SM}_\nu$ is the largest (smallest) for $M_{\eta_1} = 65$ (70) GeV, respectively.

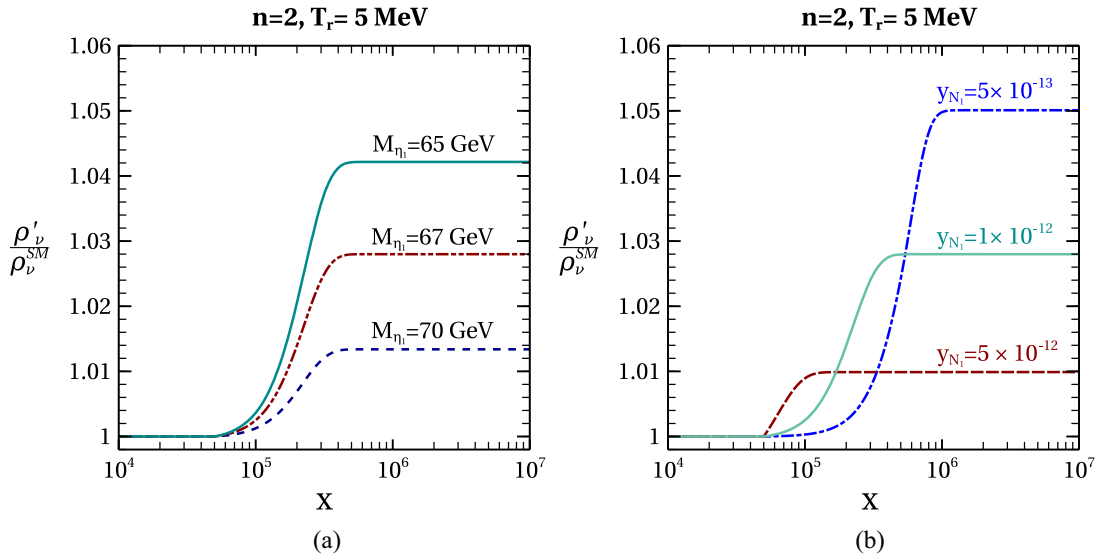

FIG. 4. Evolution of the ratio $\rho'_\nu/\rho^{\rm SM}_\nu$ as a function of x for $\lambda_3 = 10^{-3}$, $\lambda_{\phi S} = 10^{-3}$, $M_{N_1} = 10$ MeV, $\sin\theta = 0.9$, $n = 2$, $T_r = 5$ MeV. We show our findings for three different values of y_{N_1} for (a) a fixed $y_{N_1} = 10^{-12}$ and for (b) three different values of y_{N_1} for constant $M_{\eta_1} = 67$ GeV.

The Yukawa coupling y_{N_1} also controls the temperature T variation of the ratio $\rho'_\nu/\rho^{\rm SM}_\nu$ for a fixed η_1 mass. In Fig. 4(b), we show such variation of $\rho'_\nu/\rho^{\rm SM}_\nu$ with x assuming three different values of y_{N_1} (5×10^{-12}, brown dashed line; 1×10^{-12}, solid cyan line; 5×10^{-13}, blue dot-dashed line) for $M_{\eta_1} = 67$ GeV, while other parameters are the same as in Fig. 4(a). For a given mass of η_1 and N_1 and keeping other model parameters fixed, the decay of $\eta_1 \to N_1 + \nu$ is completely determined by the Yukawa coupling y_{N_1}. In addition, the larger the coupling y_{N_1}, the faster is the decay rate of η_1 and vice versa. For a given y_{N_1}, the ratio keeps on increasing with the expansion of the Universe and ultimately saturates when the decay of η_1 is completed. For any higher y_{N_1}, the aforementioned decay of η_1 gets completed even at an earlier time (equivalently, at higher temperature T) and the energy injection to the neutrino sector also completes at earlier epoch of the Universe. This phenomena is distinctly noticeable from Fig. 4(b) that the ratio saturates earlier with increase in y_{N_1}. As the higher value of the Yukawa coupling forces the η_1 decay to be completed at an earlier time, the new contribution to neutrino energy density ρ'_ν from this decay gets diluted more due to the expansion of the Universe. However, with lower Yukawa coupling $y_{N_1} = 5 \times 10^{-13}$, the decay starts later and the corresponding energy injection to neutrino sector also gets completed at a later time (lower temperature) and hence gets less diluted due to the expansion of the Universe. Consequently, one gets a higher value of $\rho'_\nu/\rho^{\rm SM}_\nu$ at lower temperature ($x \approx 10^7$) as depicted in Fig. 4(b).

After highlighting the variation of $\rho'_\nu/\rho^{\rm SM}_\nu$ with various model parameters, we now use $\rho'_\nu/\rho^{\rm SM}_\nu$ to calculate the $\Delta N_{\rm eff}$ by scanning over those model parameters and the corresponding upshot is displayed in $\Delta N_{\rm eff}$ vs M_{η_1} plane in Fig. 5. The color bar represents the value of M_{N_1} in the range 1–100 MeV. Here we consider BP-1, as the maximum allowed region from EWPD constraints correspond to this particular benchmark point. Similarly, other parameter space points satisfy the correct relic density as well being consistent with other theoretical and experimental constraints. In the calculation of $\Delta N_{\rm eff}$, we vary the DM mass

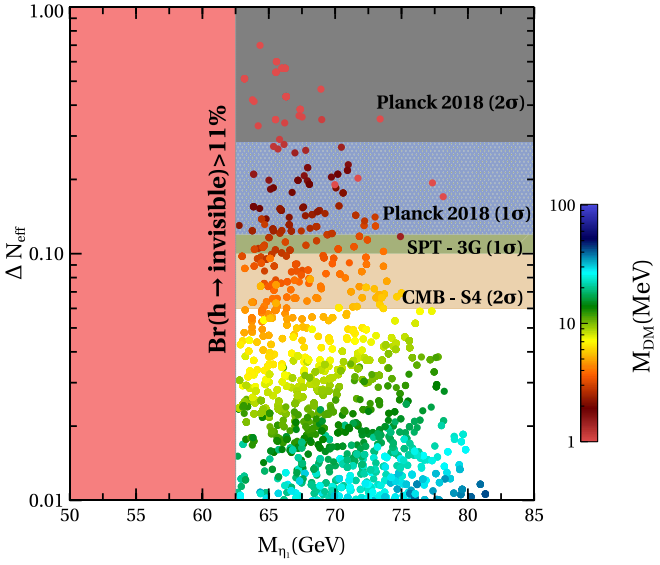

FIG. 5. Variation of $\Delta N_{\rm eff}$ with M_{η_1} for $M_{A^0} = 250$ GeV, $M_{\eta^+} = 180$ GeV, $M_{\eta_2} = 400$ GeV, $10^{-6} \le \lambda_3 \le 10^{-2}$, $10^{-6} \le \lambda_{\phi S} \le 10^{-2}$, $y_{N_1} = 10^{-12}$, $n = 2$, $T_r = 5$ MeV. The color bar in the plot represents the DM mass.

M_{N_1} from 1 to 100 MeV, and it is conspicuous from Fig. 5, that with increase in M_{N_1}, the numerical value of $\Delta N_{\rm eff}$ decreases. This is understandable, as a higher value of M_{N_1} requires lower abundance Y_{N_1} so that the correct relic density ($\Omega h^2 \sim Y_{N_1} M_{N_1}$) is achieved. In our earlier discussions, we have shown that the evolution of N_1 abundance is governed by Y_{η_1} [Fig. 2(a)]; thus lower Y_{N_1} also corresponds to smaller η_1 abundance Y_{η_1}. With this lower abundance of η_1, lesser energy gets transferred to the neutrino sector, leading to a smaller value of $\Delta N_{\rm eff}$. For this scan, we consider fixed $y_{N_1} = 10^{-12}$. We may decrease y_{N_1} that would lead an increase in $\Delta N_{\rm eff}$ as understood from Fig. 4(b) and will make the scenario more viable to the observations. However, the DM phenomenology will remain same. We also show the exclusion limit of $\Delta N_{\rm eff}$ from different present and future generation experiments. The present 2σ limit from Planck (2018) on $\Delta N_{\rm eff} = 0.285$ excludes the DM mass between ∼1 and 2 MeV, whereas the 1σ limit from Planck (2018) on $\Delta N_{\rm eff} = 0.12$ excludes DM mass in the range ∼3–4 MeV. It is also important to note that future generation experiments such as the SPT-3G [59] with 1σ limit on $\Delta N_{\rm eff} = 0.1$ and the CMB-S4 [60] with 2σ limit on $\Delta N_{\rm eff} = 0.06$ will be able to probe the DM mass up to ∼7 and ∼10 MeV, respectively. Hence, with the present and future generation experimental measurement of $\Delta N_{\rm eff}$ we can indirectly probe the freeze-in DM in this scenario and also rule out certain mass ranges of such feebly interacting dark matter.

V. SUMMARY AND CONCLUSION

We have discussed a minimal extension of the SM by an inert $SU(2)_L$ scalar doublet (η), a real scalar singlet (S), and three right-handed singlet fermions (N_1, N_2, and N_3), where all of them are odd under $\mathcal{Z}_2$ symmetry. However, the SM particles are even under the above-mentioned $\mathcal{Z}_2$ symmetry. The study has been restricted to the regime where M_{N_1} is lightest new particle in the spectrum and plays the role of a stable DM candidate. Due to the chosen $\mathcal{Z}_2$ symmetry, N_i's can only interact with SM particles through the Yukawa interaction with η and SM lepton doublet. We have assumed that the interaction of N_1 is very feeble, which is decided by the Yukawa coupling ($y_{N_1} \lesssim 10^{-12}$). Such a small interaction of N_1 prevents its production in the thermal bath. Rather, N_1 has been produced from the nonthermal decay of the long-lived lightest scalar η_1, which is one of the neutral CP-even scalar mass eigenstates obtained by diagonalizing the 2×2 mass-square matrix in (η^0, S) basis. The masses of all the other $\mathcal{Z}_2$-odd particles are sufficiently large and have no phenomenological consequences in the DM analysis. The SM neutrino masses can be generated through a one loop process via interactions of N_i and η_1 with the SM leptons. However, with such tiny Yukawa interaction, N_1 is almost decoupled from the neutrino mass generation and as a result one of the active neutrinos becomes almost massless. We have first checked the effects of different model parameters on the relic density of DM by solving the required Boltzmann equations. We have found that constraints coming from the electroweak precision data as well as the invisible decay of the SM Higgs boson ruled out a significant fraction of the model parameter space. We have seen that, in the standard radiation dominated Universe, the number densities of the mother particles (η_1) which have sizable interactions with the SM bath become smaller and have negligible impact on the $\Delta N_{\rm eff}$. On the other hand, if the early epoch of the expansion was dominated by some nonstandard species, that can change the outcome by causing faster expansion of the Universe. In this fast expanding Universe scenario, apart from producing the right amount of DM relic density, the late-time decay of η_1 can significantly impact the total radiation energy density on the start of CMB formation and puts further constraints to the allowed parameter space of the model. In order to calculate the amount of $\Delta N_{\rm eff}$, we have found the amount of energy density of neutrinos coming from the decay of η_1 by solving the required Boltzmann equation. The present 2σ limit on $\Delta N_{\rm eff}$ from Planck 2018 data excludes the DM mass as heavy as 2 MeV, as in the case of lighter DM mass, more and more energy gets converted to neutrinos and increases the value of $\Delta N_{\rm eff}$. However, future generation experiments like SPT-3G and CMB-IV will be able to probe the dark matter mass as heavy as ∼10 MeV. Thus, the analysis performed in this paper can be considered as an alternative way to probe the FIMP dark matter scenario by the precise determination of $\Delta N_{\rm eff}$ using current and future CMB data.

ACKNOWLEDGMENTS

D. N. and S. J. would like to thank D. Borah, A. Biswas, K. Dutta, S. Ganguly, D. Ghosh, and Md. I. Ali for various discussions during the project. The work of D. N. is partly supported by National Research Foundation of Korea (NRF) Grant No. 2019R1A2C3005009. The work of S. J. is supported by CSIR, Government of India, under the NET JRF fellowship scheme with File No. 09/080(1172)/2020-EMR-I.

APPENDIX: PARTICLE CONTENTS AND MODEL PARAMETERS

Particle content is given by

	$SU(2)_L$	$U(1)_Y$	Z_2
ϕ	2	$\frac{1}{2}$	+
η	2	$\frac{1}{2}$	−
S	1	0	−

The scalar potential $V(\phi,\eta,S)$ is

$$V(\phi,\eta,S) = -\mu_\phi^2(\phi^\dagger\phi) + \mu_\eta^2(\eta^\dagger\eta) + \lambda_1(\phi^\dagger\phi)^2 + \lambda_2(\eta^\dagger\eta)^2 + \mu_s^2 S^2 + \lambda_s S^4 + \lambda_3(\phi^\dagger\phi)(\eta^\dagger\eta) + \lambda_4(\phi^\dagger\eta)(\eta^\dagger\phi) + \frac{\lambda_5}{2}\{(\phi^\dagger\eta)^2 + (\eta^\dagger\phi)^2\} + \lambda_{\phi S}(\phi^\dagger\phi)S^2 + \lambda_{\eta S}(\eta^\dagger\eta)S^2 + \mu'\{(\phi^\dagger\eta)S + (\eta^\dagger\phi)S\}, \tag{A1}$$

where all parameters are real and $\mu_{i(i=\phi,\eta,s)}$ are the bare mass terms and μ' is the trilinear scalar coupling, while various quartic scalar couplings are represented by $\lambda_{i(i=1-5)}$, $\lambda_{\phi S}$, and $\lambda_{\eta S}$, respectively. We write the SM scalar doublet as

$$\phi = \frac{1}{\sqrt{2}}\begin{bmatrix}\phi_1 + i\phi_2 \\ \phi_3 + i\phi_4\end{bmatrix}, \tag{A2}$$

where ϕ_i are real. From the minimization condition of the potential V in Eq. (A1), we get

$$\phi_j\left(-\mu_\phi^2 + \lambda_1\sum_i^4 \phi_i^2\right) = 0. \tag{A3}$$

Any point on the circle $(-\mu_\phi^2 + \lambda_1\sum_i^4\phi^2) = 0$ is a local minimum of the potential in Eq. (A1) and choosing a particular point $(\phi_1 = \phi_2 = \phi_4 = 0, \phi_3 = v = \sqrt{\mu_\phi^2/\lambda_1})$ will spontaneously break the symmetry. After the spontaneous symmetry breaking of the SM Higgs doublet, the doublet scalars can be represented as follows:

$$\phi = \begin{bmatrix}0 \\ \frac{v+h}{\sqrt{2}}\end{bmatrix}, \qquad \eta = \begin{bmatrix}\eta^\pm \\ \frac{\eta^0 + iA^0}{\sqrt{2}}\end{bmatrix}, \tag{A4}$$

where $v = 246$ GeV is the SM electroweak vacuum expectation value. The masses of the SM-like Higgs (h) and the charged scalar ($\eta^\pm$) and the pseudoscalar particles (A^0) can be written as

$$M_h^2 = 2\lambda_1 v^2, \tag{A5}$$

$$M_{\eta^\pm}^2 = \mu_\eta^2 + \frac{\lambda_3}{2}v^2, \tag{A6}$$

$$M_{A^0}^2 = \mu_\eta^2 + (\lambda_3 + \lambda_4 - \lambda_5)\frac{v^2}{2}. \tag{A7}$$

Due to the presence of the trilinear interaction $(\phi^\dagger\eta S)$ in the scalar potential, the neutral CP-even component η^0 mixes with the real singlet scalar S, and the corresponding mass-square matrix in (η^0, S) basis has the following form:

$$M_{\eta^0 S}^2 = \begin{bmatrix}\frac{\partial^2 V}{\partial\eta^{0^2}} & \frac{\partial^2 V}{\partial\eta^0\partial S} \\ \frac{\partial^2 V}{\partial\eta^0\partial S} & \frac{\partial^2 V}{\partial S^2}\end{bmatrix} = \begin{bmatrix}\mu_\eta^2 + \lambda_L v^2 & v\mu' \\ v\mu' & 2\mu_s^2 + \lambda_{\phi S}v^2\end{bmatrix}, \tag{A8}$$

where $\lambda_L = \frac{1}{2}(\lambda_3 + \lambda_4 + \lambda_5)$. The eigenvalues and CP-even neutral physical eigenstates can be obtained by diagonalizing the above mass-squared matrix,

$$M_{\eta_1\eta_2}^2 = O^T M_{\eta^0 S}^2 O, \tag{A9}$$

where

$$O = \begin{bmatrix}\cos\theta & \sin\theta \\ -\sin\theta & \cos\theta\end{bmatrix}, \tag{A10}$$

and $M_{\eta_1\eta_2}^2$ is given by

$$M_{\eta_1\eta_2}^2 = \begin{bmatrix}M_{\eta_1}^2 & 0 \\ 0 & M_{\eta_2}^2\end{bmatrix}. \tag{A11}$$

The corresponding eigenstates η_1 and η_2 are given in terms of the weak basis (η^0, S) and the mixing angle θ,

$$\eta_1 = \eta^0\cos\theta - S\sin\theta, \tag{A12}$$

$$\eta_2 = \eta^0\sin\theta + S\cos\theta. \tag{A13}$$

The free parameters of the scalar sectors are the following: M_{η_1}, M_{η_2}, $M_{\eta^\pm}$, M_{A^0}, λ_η, λ_S, $\lambda_{\phi S}$, $\lambda_{\eta S}$, λ_3, and $\sin\theta$. We set the SM-like Higgs boson mass $M_h = 125$ GeV throughout this analysis. All other parameters of the scalar sector can be expressed in terms of those free parameters. From Eqs. (A8)–(A11), we get the following relations:

$$\mu_\eta^2 = \cos^2\theta M_{\eta_1}^2 + \sin^2\theta M_{\eta_2}^2 - \lambda_L v^2, \tag{A14}$$

$$\mu' = \cos\theta\sin\theta\frac{1}{v}(M_{\eta_2}^2 - M_{\eta_1}^2), \tag{A15}$$

$$\mu_s^2 = \frac{1}{2}(\sin^2\theta M_{\eta_1}^2 + \cos^2\theta M_{\eta_2}^2 - \lambda_{\phi S}v^2). \tag{A16}$$

Substituting these parameters in scalar masses in Eq. (A7), we get

$$\lambda_5 = \frac{1}{v^2}(\cos^2\theta M_{\eta_1}^2 + \sin^2\theta M_{\eta_2}^2 - M_{A^0}^2), \tag{A17}$$

$$\lambda_4 + \lambda_5 = \frac{2}{v^2}(\cos^2\theta M_{\eta_1}^2 + \sin^2\theta M_{\eta_2}^2 - M_{\eta^+}^2). \tag{A18}$$

Now we have written the dependent parameters $(\mu_\eta, \mu', \mu_S, \lambda_4, \lambda_5)$ in terms of free parameters.

[1] T2K Collaboration, Indication of Electron Neutrino Appearance from an Accelerator-Produced Off-Axis Muon Neutrino Beam, Phys. Rev. Lett. **107**, 041801 (2011).

[2] Double Chooz Collaboration, Indication of Reactor $\bar{\nu}_e$ Disappearance in the Double Chooz Experiment, Phys. Rev. Lett. **108**, 131801 (2012).

[3] Daya Bay Collaboration, Observation of Electron-Antineutrino Disappearance at Daya Bay, Phys. Rev. Lett. **108**, 171803 (2012).

[4] RENO Collaboration, Observation of Reactor Electron Antineutrino Disappearance in the RENO Experiment, Phys. Rev. Lett. **108**, 191802 (2012).

[5] MINOS Collaboration, Electron Neutrino and Antineutrino Appearance in the Full MINOS Data Sample, Phys. Rev. Lett. **110**, 171801 (2013).

[6] Particle Data Group Collaboration, Review of particle physics, Prog. Theor. Exp. Phys. **2020**, 083C01 (2020).

[7] F. Zwicky, Die Rotverschiebung von extragalaktischen Nebeln, Helv. Phys. Acta **6**, 110 (1933).

[8] V. C. Rubin and W. K. Ford, Jr., Rotation of the Andromeda nebula from a spectroscopic survey of emission regions, Astrophys. J. **159**, 379 (1970).

[9] D. Clowe, M. Bradac, A. H. Gonzalez, M. Markevitch, S. W. Randall, C. Jones, and D. Zaritsky, A direct empirical proof of the existence of dark matter, Astrophys. J. Lett. **648**, L109 (2006).

[10] Planck Collaboration, Planck 2018 results. VI. Cosmological parameters, Astron. Astrophys. **641**, A6 (2020).

[11] P. Minkowski, $\mu \to e\gamma$ at a rate of one out of 10^9 muon decays?, Phys. Lett. **67B**, 421 (1977).

[12] R. N. Mohapatra and G. Senjanovic, Neutrino Mass and Spontaneous Parity Nonconservation, Phys. Rev. Lett. **44**, 912 (1980).

[13] J. Schechter and J. W. F. Valle, Neutrino masses in $SU(2) \times U(1)$ theories, Phys. Rev. D **22**, 2227 (1980).

[14] M. Gell-Mann, P. Ramond, and R. Slansky, Complex spinors and unified theories, Conf. Proc. C **790927**, 315 (1979).

[15] R. N. Mohapatra and G. Senjanovic, Neutrino masses and mixings in gauge models with spontaneous parity violation, Phys. Rev. D **23**, 165 (1981).

[16] G. Lazarides, Q. Shafi, and C. Wetterich, Proton lifetime and fermion masses in an SO(10) model, Nucl. Phys. **B181**, 287 (1981).

[17] C. Wetterich, Neutrino masses and the scale of B-L violation, Nucl. Phys. **B187**, 343 (1981).

[18] J. Schechter and J. W. F. Valle, Neutrino decay and spontaneous violation of lepton number, Phys. Rev. D **25**, 774 (1982).

[19] B. Brahmachari and R. N. Mohapatra, Unified explanation of the solar and atmospheric neutrino puzzles in a minimal supersymmetric SO(10) model, Phys. Rev. D **58**, 015001 (1998).

[20] R. Foot, H. Lew, X. G. He, and G. C. Joshi, Seesaw neutrino masses induced by a triplet of leptons, Z. Phys. C **44**, 441 (1989).

[21] E. Ma, Pathways to Naturally Small Neutrino Masses, Phys. Rev. Lett. **81**, 1171 (1998).

[22] E. Ma, Verifiable radiative seesaw mechanism of neutrino mass and dark matter, Phys. Rev. D **73**, 077301 (2006).

[23] E. W. Kolb and M. S. Turner, *The Early Universe* (CRC Press, Boca Raton, 1990), Vol. 69.

[24] J. L. Feng, Dark matter candidates from particle physics and methods of detection, Annu. Rev. Astron. Astrophys. **48**, 495 (2010).

[25] L. Roszkowski, E. M. Sessolo, and S. Trojanowski, WIMP dark matter candidates and searches—current status and future prospects, Rep. Prog. Phys. **81**, 066201 (2018).

[26] M. Schumann, Direct detection of WIMP dark matter: Concepts and status, J. Phys. G **46**, 103003 (2019).

[27] T. Lin, Dark matter models and direct detection, Proc. Sci. 333 (**2019**) 009.

[28] G. Arcadi, M. Dutra, P. Ghosh, M. Lindner, Y. Mambrini, M. Pierre, S.Profumo, and F. S. Queiroz, The waning of the WIMP? A review of models, searches, and constraints, Eur. Phys. J. C **78**, 203 (2018).

[29] PandaX-II Collaboration, Dark Matter Results from First 98.7 Days of Data from the PandaX-II Experiment, Phys. Rev. Lett. **117**, 121303 (2016).

[30] XENON Collaboration, First Dark Matter Search Results from the XENON1T Experiment, Phys. Rev. Lett. **119**, 181301 (2017).

[31] LUX Collaboration, Results from a Search for Dark Matter in the Complete LUX Exposure, Phys. Rev. Lett. **118**, 021303 (2017).

[32] PICO Collaboration, Dark matter search results from the complete exposure of the PICO-60 C_3F_8 bubble chamber, Phys. Rev. D **100**, 022001 (2019).

[33] AMS Collaboration, First Result from the Alpha Magnetic Spectrometer on the International Space Station: Precision Measurement of the Positron Fraction in Primary Cosmic Rays of 0.5–350 GeV, Phys. Rev. Lett. **110**, 141102 (2013).

[34] J. Buckley *et al.*, Working group report: WIMP dark matter indirect detection, arXiv:1310.7040.

[35] J. M. Gaskins, A review of indirect searches for particle dark matter, Contemp. Phys. **57**, 496 (2016).

[36] Fermi-LAT and DES Collaborations, Searching for dark matter annihilation in recently discovered Milky Way satellites with Fermi-LAT, Astrophys. J. **834**, 110 (2017).

[37] MAGIC and Fermi-LAT Collaboration, Limits to dark matter annihilation cross-section from a combined analysis of MAGIC and Fermi-LAT observations of dwarf satellite galaxies, J. Cosmol. Astropart. Phys. 02 (2016) 039.

[38] T. Bringmann and C. Weniger, Gamma ray signals from dark matter: Concepts, status and prospects, Phys. Dark Universe **1**, 194 (2012).

[39] M. Cirelli, Status of indirect (and direct) dark matter searches, Proc. Sci. ICRC2015 (**2016**) 014.

[40] F. Kahlhoefer, Review of LHC dark matter searches, Int. J. Mod. Phys. A **32**, 1730006 (2017).

[41] A. Boveia and C. Doglioni, Dark matter searches at colliders, Annu. Rev. Nucl. Part. Sci. **68**, 429 (2018).

[42] L. J. Hall, K. Jedamzik, J. March-Russell, and S. M. West, Freeze-in production of FIMP dark matter, J. High Energy Phys. 03 (2010) 080.

[43] J. König, A. Merle, and M. Totzauer, keV sterile neutrino dark matter from singlet scalar decays: The most general case, J. Cosmol. Astropart. Phys. 11 (2016) 038.

[44] A. Biswas and A. Gupta, Freeze-in production of sterile neutrino dark matter in $U(1)_{B-L}$ model, J. Cosmol. Astropart. Phys. 09 (2016) 044.

[45] A. Biswas and A. Gupta, Calculation of momentum distribution function of a non-thermal fermionic dark matter, J. Cosmol. Astropart. Phys. 03 (2017) 033.

[46] N. Bernal, M. Heikinheimo, T. Tenkanen, K. Tuominen, and V. Vaskonen, The dawn of FIMP dark matter: A review of models and constraints, Int. J. Mod. Phys. A **32**, 1730023 (2017).

[47] D. Borah, B. Karmakar, and D. Nanda, Common origin of dirac neutrino mass and freeze-in massive particle dark matter, J. Cosmol. Astropart. Phys. 07 (2018) 039.

[48] J. Heeck and D. Teresi, Cold keV dark matter from decays and scatterings, Phys. Rev. D **96**, 035018 (2017).

[49] K. J. Bae, A. Kamada, S. P. Liew, and K. Yanagi, Light axinos from freeze-in: Production processes, phase space distributions, and Ly-α forest constraints, J. Cosmol. Astropart. Phys. 01 (2018) 054.

[50] S. Boulebnane, J. Heeck, A. Nguyen, and D. Teresi, Cold light dark matter in extended seesaw models, J. Cosmol. Astropart. Phys. 04 (2018) 006.

[51] G. Ballesteros, M. A. G. Garcia, and M. Pierre, How warm are non-thermal relics? Lyman-α bounds on out-of-equilibrium dark matter, J. Cosmol. Astropart. Phys. 03 (2021) 101.

[52] F. D'Eramo and A. Lenoci, Lower mass bounds on FIMP dark matter produced via freeze-in, J. Cosmol. Astropart. Phys. 10 (2021) 045.

[53] Q. Decant, J. Heisig, D. C. Hooper, and L. Lopez-Honorez, Lyman-α constraints on freeze-in and superWIMPs, J. Cosmol. Astropart. Phys. 03 (**2022**) 041.

[54] S.-P. Li, X.-Q. Li, X.-S. Yan, and Y.-D. Yang, Simple estimate of BBN sensitivity to light freeze-in dark matter, Phys. Rev. D **104**, 115007 (2021).

[55] S. Ganguly, S. Roy, and A. K. Saha, Imprints of MeV scale hidden dark sector at Planck, Phys. Lett. B **834**, 137463 (2022).

[56] G. Mangano, G. Miele, S. Pastor, T. Pinto, O. Pisanti, and P. D. Serpico, Relic neutrino decoupling including flavor oscillations, Nucl. Phys. **B729**, 221 (2005).

[57] E. Grohs, G. M. Fuller, C. T. Kishimoto, M. W. Paris, and A. Vlasenko, Neutrino energy transport in weak decoupling and big bang nucleosynthesis, Phys. Rev. D **93**, 083522 (2016).

[58] P. F. de Salas and S. Pastor, Relic neutrino decoupling with flavour oscillations revisited, J. Cosmol. Astropart. Phys. 07 (2016) 051.

[59] SPT-3G Collaboration, Particle physics with the cosmic microwave background with SPT-3G, J. Phys. Conf. Ser. **1468**, 012008 (2020).

[60] CMB-S4 Collaboration, CMB-S4 science book, first edition, arXiv:1610.02743.

[61] M. Kawasaki, K. Kohri, and N. Sugiyama, MeV scale reheating temperature and thermalization of neutrino background, Phys. Rev. D **62**, 023506 (2000).

[62] K. Ichikawa, M. Kawasaki, and F. Takahashi, The oscillation effects on thermalization of the neutrinos in the Universe with low reheating temperature, Phys. Rev. D **72**, 043522 (2005).

[63] F. D'Eramo, N. Fernandez, and S. Profumo, When the Universe expands too fast: Relentless dark matter, J. Cosmol. Astropart. Phys. 05 (**2017**) 012.

[64] M. Joyce, Electroweak baryogenesis and the expansion rate of the Universe, Phys. Rev. D **55**, 1875 (1997).

[65] M. S. Turner, Coherent scalar field oscillations in an expanding Universe, Phys. Rev. D **28**, 1243 (1983).

[66] D. Wands, E. J. Copeland, and A. R. Liddle, Exponential potentials, scaling solutions and inflation, in *Proceedings of the 16th Texas Symposium on Relativistic Astrophysics and 3rd Particles, Strings, and Cosmology Symposium* (1993), pp. 0647–652.

[67] B. Ratra and P. J. E. Peebles, Cosmological consequences of a rolling homogeneous scalar field, Phys. Rev. D **37**, 3406 (1988).

[68] E. J. Copeland, A. R. Liddle, and D. Wands, Exponential potentials and cosmological scaling solutions, Phys. Rev. D **57**, 4686 (1998).

[69] N. Bernal, C. Cosme, T. Tenkanen, and V. Vaskonen, Scalar singlet dark matter in non-standard cosmologies, Eur. Phys. J. C **79**, 30 (2019).

[70] A. Poulin, Dark matter freeze-out in modified cosmological scenarios, Phys. Rev. D **100**, 043022 (2019).

[71] K. Redmond and A. L. Erickcek, New constraints on dark matter production during kination, Phys. Rev. D **96**, 043511 (2017).

[72] E. Hardy, Higgs portal dark matter in non-standard cosmological histories, J. High Energy Phys. 06 (2018) 043.

[73] B. Barman, P. Ghosh, F. S. Queiroz, and A. K. Saha, Scalar multiplet dark matter in a fast expanding Universe: Resurrection of the desert region, Phys. Rev. D **104**, 015040 (2021).

[74] F. D'Eramo, N. Fernandez, and S. Profumo, Dark matter freeze-in production in fast-expanding universes, J. Cosmol. Astropart. Phys. 02 (2018) 046.

[75] R. T. Co, F. D'Eramo, L. J. Hall, and D. Pappadopulo, Freeze-in dark matter with displaced signatures at colliders, J. Cosmol. Astropart. Phys. 12 (2015) 024.

[76] A. Berlin, D. Hooper, and G. Krnjaic, PeV-scale dark matter as a thermal relic of a decoupled sector, Phys. Lett. B **760**, 106 (2016).

[77] T. Tenkanen and V. Vaskonen, Reheating the Standard Model from a hidden sector, Phys. Rev. D **94**, 083516 (2016).

[78] J. A. Dror, E. Kuflik, and W. H. Ng, Codecaying Dark Matter, Phys. Rev. Lett. **117**, 211801 (2016).

[79] A. Berlin, D. Hooper, and G. Krnjaic, Thermal dark matter from a highly decoupled sector, Phys. Rev. D **94**, 095019 (2016).

[80] D. Borah, P. S. B. Dev, and A. Kumar, TeV scale leptogenesis, inflaton dark matter and neutrino mass in a scotogenic model, Phys. Rev. D **99**, 055012 (2019).

[81] T. Kitabayashi, Primordial black holes and scotogenic dark matter, Int. J. Mod. Phys. A **36**, 2150139 (2021).

[82] V. De Romeri, M. Puerta, and A. Vicente, Dark matter in a charged variant of the Scotogenic model, Eur. Phys. J. C **82**, 623 (2022).

[83] P. Escribano and A. Vicente, An ultraviolet completion for the scotogenic model, Phys. Lett. B **823**, 136717 (2021).

[84] I. M. Ávila, G. Cottin, and M. A. Díaz, Revisiting the scotogenic model with scalar dark matter, J. Phys. G **49**, 065001 (2022).
[85] A. Alvarez, R. Cepedello, M. Hirsch, and W. Porod, Temperature effects on the Z2 symmetry breaking in the scotogenic model, Phys. Rev. D **105**, 035013 (2022).
[86] P. Escribano, A generalization of the Scotogenic model, J. Phys. Conf. Ser. **2156**, 012099 (2021).
[87] R. S. Hundi, Lepton flavor violating Z and Higgs decays in the scotogenic model, Eur. Phys. J. C **82**, 505 (2022).
[88] N. G. Deshpande and E. Ma, Pattern of symmetry breaking with two Higgs doublets, Phys. Rev. D **18**, 2574 (1978).
[89] R. Barbieri, L. J. Hall, and V. S. Rychkov, Improved naturalness with a heavy Higgs: An alternative road to LHC physics, Phys. Rev. D **74**, 015007 (2006).
[90] L. Lopez Honorez, E. Nezri, J. F. Oliver, and M. H. G. Tytgat, The inert doublet model: An archetype for dark matter, J. Cosmol. Astropart. Phys. 02 (2007) 028.
[91] A. Arhrib, Y.-L. S. Tsai, Q. Yuan, and T.-C. Yuan, An updated analysis of inert Higgs doublet model in light of the recent results from LUX, PLANCK, AMS-02 and LHC, J. Cosmol. Astropart. Phys. 06 (2014) 030.
[92] A. Beniwal, J. Herrero-García, N. Leerdam, M. White, and A. G. Williams, The scotoSinglet model: A scalar singlet extension of the scotogenic model, J. High Energy Phys. 06 (2021) 136.
[93] Y. Farzan, A minimal model linking two great mysteries: Neutrino mass and dark matter, Phys. Rev. D **80**, 073009 (2009).
[94] A. Ahriche, K. L. McDonald, and S. Nasri, The scale-invariant scotogenic model, J. High Energy Phys. 06 (2016) 182.
[95] A. Biswas, D. Borah, and D. Nanda, Light dirac neutrino portal dark matter with observable ΔNeff, J. Cosmol. Astropart. Phys. 10 (2021) 002.
[96] P. G. Ferreira and M. Joyce, Cosmology with a primordial scaling field, Phys. Rev. D **58**, 023503 (1998).
[97] P. G. Ferreira and M. Joyce, Structure Formation with a Self-Tuning Scalar Field, Phys. Rev. Lett. **79**, 4740 (1997).
[98] R. Kallosh and A. Linde, Universality class in conformal inflation, J. Cosmol. Astropart. Phys. 07 (2013) 002.
[99] R. Kallosh, A. Linde, and D. Roest, Superconformal inflationary α-attractors, J. High Energy Phys. 11 (2013) 198.
[100] A. Starobinsky, A new type of isotropic cosmological models without singularity, Phys. Lett. **91B**, 99 (1980).
[101] L. Kofman, A. Linde, and A. Starobinsky, Inflationary universe generated by the combined action of a scalar field and gravitational vacuum polarization, Phys. Lett. **157B**, 361 (1985).
[102] R. R. Caldwell, R. Dave, and P. J. Steinhardt, Cosmological Imprint of an Energy Component with General Equation of State, Phys. Rev. Lett. **80**, 1582 (1998).
[103] C. Wetterich, The cosmon model for an asymptotically vanishing time dependent cosmological 'constant', Astron. Astrophys. **301**, 321 (1995).
[104] V. Sahni and A. A. Starobinsky, The case for a positive cosmological Lambda term, Int. J. Mod. Phys. D **09**, 373 (2000).
[105] A. Alloul, N. D. Christensen, C. Degrande, C. Duhr, and B. Fuks, FeynRules 2.0—A complete toolbox for tree-level phenomenology, Comput. Phys. Commun. **185**, 2250 (2014).
[106] A. Belyaev, N. D. Christensen, and A. Pukhov, CALCHEP 3.4 for collider physics within and beyond the Standard Model, Comput. Phys. Commun. **184**, 1729 (2013).
[107] G. Bélanger, F. Boudjema, A. Pukhov, and A. Semenov, micrOMEGAs4.1: Two dark matter candidates, Comput. Phys. Commun. **192**, 322 (2015).
[108] K. Kannike, Vacuum stability conditions from copositivity criteria, Eur. Phys. J. C **72**, 2093 (2012).
[109] M. E. Peskin and T. Takeuchi, Estimation of oblique electroweak corrections, Phys. Rev. D **46**, 381 (1992).
[110] H. E. Haber and D. O'Neil, Basis-independent methods for the two-Higgs-doublet model III: The CP-conserving limit, custodial symmetry, and the oblique parameters S, T, U, Phys. Rev. D **83**, 055017 (2011).
[111] ATLAS Collaboration, Combination of Searches for Invisible Higgs Boson Decays with the ATLAS Experiment, Phys. Rev. Lett. **122**, 231801 (2019).